

# Measuring and Calculation of Positive Corona Currents Using Comsol Multiphysics

M. Quast, N.R. Lalic

Gunytronic Gasflow Sensoric Systems GmbH, Langenharter Straße 20, 4300 St. Valentin

[m.quast@gunytronic.com](mailto:m.quast@gunytronic.com)

[n.lalic@gunytronic.com](mailto:n.lalic@gunytronic.com)

## Abstract:

The sensor type developed by Gunytronic uses corona discharge for measuring flow rates in exhaust streams of automotives, aircrafts and industrial plants. This paper will present the development of testing equipment used in laboratory for investigating physical relations on corona currents, charged particle transport, the calculation of the collateral electric fields and high potentials. This enhanced understanding of the nature of corona currents was used to improve the geometry of the sensor system. Improving the sensor properties will be issue of another paper, which will be published soon. Here we will give some deeper insight in the collaboration of mathematical simulation and physical experimental work in the lab and vice versa.

**Keywords:** corona current, plasma physics, plasma chemistry, ion wind, electric potential, electric field, pin plate configuration

## 1. Introduction

Air always contains a varying amount of electrons due to cosmic radiation and UV light. This causes a slight negative electric field in lower atmosphere. When applying a strong electric field, one can observe the well established phenomena known as electric breakdown, streamer discharge, glow discharge and corona discharge.

### 1.1 The physics of corona phenomena

In the centre of attraction one can find a sharp needle set under high positive voltage (anode). The tip is placed opposite to two squared flat metal plates on ground (collector). This configuration is the standard experimental set up for experiments on any corona phenomena. The electric field forces the uniformly distributed electrons towards the tip. The electrons collide

with neutral gas molecules and dependent upon their energy high energy electrons produce positive ions while low energy electrons result in negative ions because of attachment reactions. The positive charged particles accelerated in the electric field towards the collector and also colliding with neutral gas species just transfer momentum and energy to these neutrals causing a wind downwards to the collector. We calculated wind speeds of approximately 6-10 m/s, which we also measured in experiment. There is also a wind generated upwards due to momentum transfer of negative ions to neutrals, which can be calculated but it is too weak to be measured with our instrumentation. The so called ionization zone, a blue shimmering region sending out high energetic UV light because of recombination reactions of positive ions and electrons, is located near to the tip.



**Figure1.** Corona light in a needle tip-plate configuration for different needle materials: gold, aluminum, silver, steel, diamond coated steel and tungsten. The grounded plates all are made of copper.

As most kinetic energy and momentum is transferred to neutrals the charge distribution is concentrated in two main regions. In the drift zone, between needle and metal plate electrons, positive and negative molecules are concentrated in a cone shaped volume as seen in figures 1 and 2.

Alongside the metal plates the charge distribution will be more or less of Warburg type, described by equations (1) and (2):

$$(eq.1) \quad J(\theta) = J_w(0) \cos^n(\theta)$$

$$(eq.2) \quad J_w(0) = \frac{k_w V(V-V_i)}{dP}$$

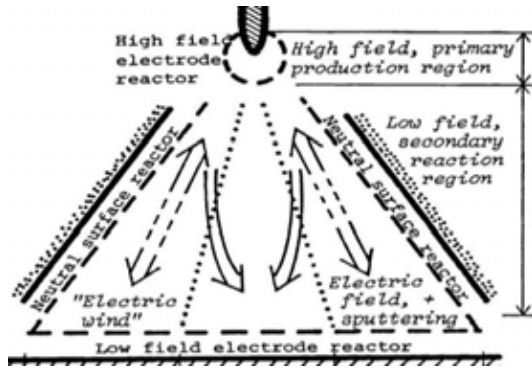


**Figure2.** Sketch of corona transport regions: the lower regions are dominated by attachment reactions, the higher regions are dominated by positive ions and electrons

here:  $J(\theta)$  is the current density,  $\theta$  is the opening angle,  $V$  is the tip voltage,  $V_i$  is the corona onset Voltage,  $d$  is the distance between tip and plate,  $k_w$  and  $p$  are fitting parameters.

According to figure3 the Warburg distribution mainly depends on the opening angle  $\theta$ , the voltage difference between the tip voltage  $V$  and the corona onset voltage  $V_i$ . The coefficient  $k_w = 8.11 \cdot 10^{-14}$  was found experimentally and the dimensionless numbers  $p = 2 \dots 3$  and  $n = 4.5 \dots 6$  were found by others before [8,9,11], depending on the geometry of the plates.

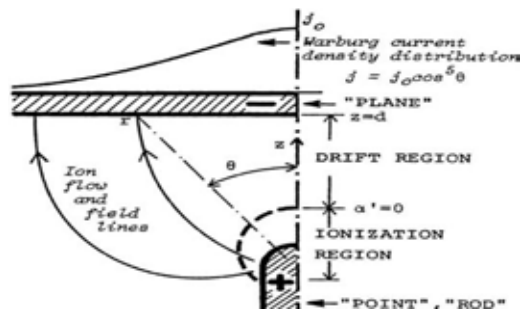


**Figure3.** Sketch of Warburg like  $\cos^n \theta$  current distribution. Warburg theory finds that the exponent  $n$  should be exactly 5, while in experiment the exponent differs from 4.5 to 6.

## 2. Experimental Setup

The testing apparatus which is shown in figures 4 and 5 consists of two Teflon plates of about 50 cm diameter. These plates protect the metal plates and needle from dust particles. A Teflon fastener fixes the needle in the mid position. A step motor can move the upper part of the construction up and down. An additional motor can turn the set up by  $360^\circ$  around the symmetry axis. For the following simulation and verifying of the calculation the distance between the tip and the metal plates is being kept constant at  $d = 27$  mm. The whole plant is covered and protected by a Plexiglas box. The metal plates were fabricated by etching a conductor board. The separation distance between the two plates is 1 mm. In addition the copper plates have been chemically coated with gold.

The gas inside the box is air. The temperature, moisture and pressure have been measured but not controlled, these parameters lie within a range of  $21.5 - 23.5$  °C, 41-45%, 967-998 mbar during experiment. The voltage on the anode can be changed from 0 to 10 kV continuously.

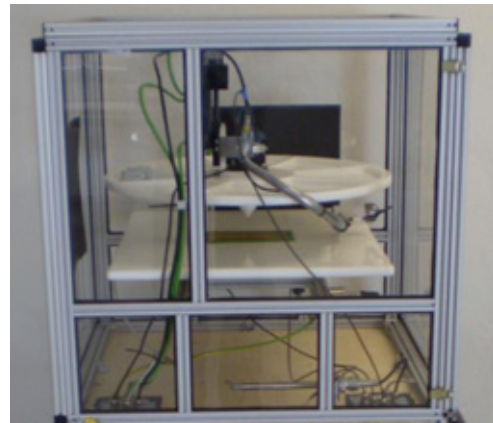


**Figure4.** The experimental setup for measuring corona currents is being protected by a Plexiglas box.

After having reached an onset voltage of about 3500 Volts two corona currents can be measured on the copper plates. Gunytronic developed this testing systems using COMSOL Multiphysics (CM) to predict the corona current on the two plates.

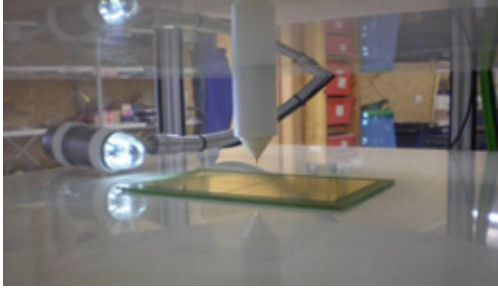


**Figure5.** Needle used for producing corona plasma and two copper plates for measuring currents is fixed in the white Teflon fastener. The normal distance from the tip to the plates in the experiment is 27 mm. A camera can be used optionally to take photos.

### 3. Multiphysics Modelling

#### 3.1 Governing Equations

The main idea for the geometry and the mathematical model was taken from [1]. The drawing in figure6 shows a simple 2D model. In the red highlighted triangular subdomain most charges are transported to the plates.

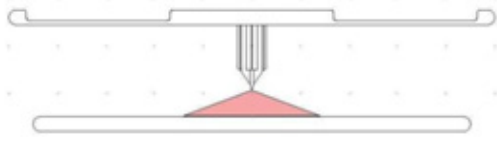


**Figure6.** Model used for FEM calculation of corona currents on two thin copper plates due to a high driving voltage on a sharp tip 27 mm above the plates.

We assume that the potential on the tip of the needle is positive. Positive Ions are therefore repelled and flow downward, while negative charged ions and electrons move upward. For modeling the corona current in a steady state regime we used the following transport equation included in the CM chemical engineering toolbox:

$$(eq.3) \quad \nabla \cdot (cu - zKc\nabla V - D\nabla c) = 0$$

In a small ball around the tip of the needle we set the initial concentration of ions  $c$  ( $\text{mol}/\text{m}^3$ ) to  $c \sim N_L \cdot 10^{-9}$ , where  $N_L = 2.687 \cdot 10^{25} \text{ m}^{-3}$  is Loschmidt's number. The concentration  $c$  of the species is also the coupling variable to the Poisson equation and the charge density  $\rho_0$

(eq4.). The coupling was done by multiplying  $c$  with the Faraday constant  $96485.339 \text{ (9) C/mol}$ . The velocity  $u$  is the resulting velocity from the local side wind of about  $1 \text{ m/s}$  and the ionic wind velocity of  $6 \text{ m/s}$ . The number of charges per molecule is  $z$  and was always set to one, as we assumed double ionization to be insignificant. The ion mobility is represented by  $K = 2.2 \cdot 10^{-4} \text{ m}^2/\text{Vs}$  and the diffusion of ions in air by  $D = 5.686 \cdot 10^{-6} \text{ m}^2/\text{s}$ .  $V$  is the applied electric potential on the surface of the tip. These equations connect the physics of ion motion in the electric field and the ion transport by conduction. CM is used to calculate the ionic current on the copper plates. These measurements are then compared with the results of the testing equipment. To calculate the electric field we modified the Poisson equation the following way:

$$(eq.4) \quad \nabla \cdot \left( \left( \sigma + \frac{\epsilon_0 \epsilon}{T} \right) \nabla V - J^e \right) = \frac{\rho_0}{T}$$

where:  $\sigma$  is the electrical conductivity of the triangular subdomain,  $\epsilon$  is the relative electric permittivity of air (1.0003 for almost all gaseous species) and  $\epsilon_0$  is the permittivity of vacuum. The external current density  $J^e$  is zero. The initial value of the charge density  $\rho_0$  is set zero to calculate the electric field without transport of current carriers. The generalized electrostatic mode defines the parameter  $T$ . Although in the later versions of CM the generalized electrostatic mode was removed, we could prove it in various experiments to be of sufficient reliability for setting up our model.

After the calculation of the electric field we calculated the coupling between space charge density and space charge transport. In this Model we calculate the transport of charges due to electric field and diffusion just for one ion species as we assumed the chemical reaction in the plasma ball should be in equilibrium and just being dominated by one ion sort. The results for more than one ion species using a three phase hydrodynamic plasma model will be presented by Gunytronic on the CM Conference 2009 as a poster and as a paper in these conference proceedings.

### 3.2 Subdomain and boundary conditions

Within the highlighted subdomain in figure 6, a variable conductivity has been assumed. The following function to model the conductivity of air was found experimentally:

$$(eq.5) \quad \sigma := \frac{1.89 \cdot 10^{-13}}{d^{3+f}} \cdot \left[ \left( \frac{V-3800}{1000} \cdot 0.000245 - 0.0005 \right) \right]$$

$\sigma$  changes with the voltage  $V$ , the distance  $d$  is set to 27 mm. We assumed the corona set up being an electric dipole. Therefore, we used idea of an electric potential of a dipole field decreasing proportional to  $\approx 1/d^3$ . The number  $f$  is a correcting exponent since the needle not an ideal dipole. We also assumed that there should be a linear relation between current and voltage. That is the reason for the numbers 0.000245, 0.0005 and  $1.89 \cdot 10^{-13}$ , which are just coefficients of a linear equation. The subdomain conditions of the remaining subdomains shown in figure 6 are as follows:

Material	$\sigma$	$\epsilon$
Copper	$5.99e10^7$	$\infty$
Iron/steal	$1.50e10^6$	$\infty$
Teflon	$-\infty$	2.1

The symbol “ $\infty$ ” is a variable for very small or high numbers to keep the calculation stable. The outermost boundary simulating the Plexiglas box is set on electric insulation. Other boundaries are set on ground in the case of being conductors or on zero charge in the case of being non conducting dielectric materials. We solved the model using a parametric solver, increasing the tip voltage from 0 to 10000 V in 100 V steps.

### 4. Results

In figure7 there is shown the voltage current diagram during a corona experiment solved with a parametric solver for voltages from 0 to 10 kV. As we increase the voltage the corona current starts to flow at about 3800 V onset voltage. This value we used for calculating and predicting the corona current. The simulation results deviate from the experiment less than 10 % for voltages between the onset level and the maximum voltage of 10 kV.

The same method was used to calculate the Warburg distribution of the electric current. This

result can be seen in figure8, which shows the corona current as a function of the needle's deviation from the symmetry axis. The experimental data and the simulation data fit within an error tolerance of +/- 10%.

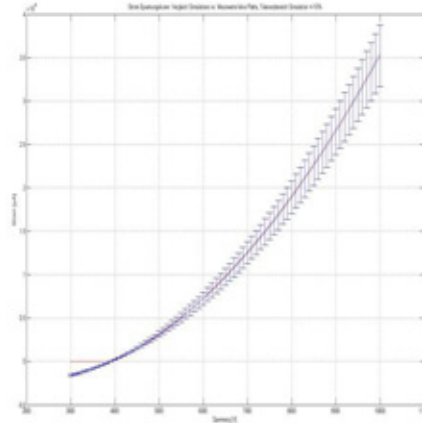


**Figure7.** Corona voltage current relation comparison of experimental and calculated data.

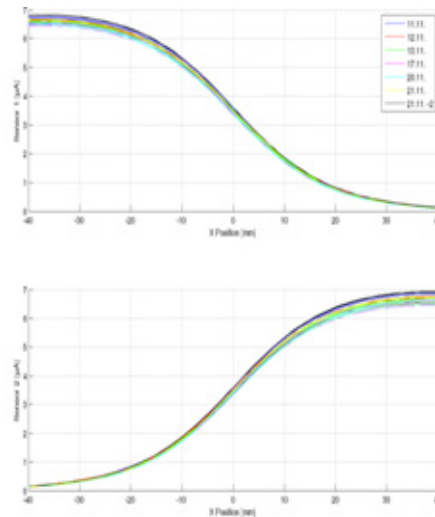


**Figure8.** Proof of the Warburg distribution with CM FEM methods. The Experiment was rerun seven times during at different daytimes and days. The upper graph shows the current distribution for the right plate the lower graph for left plate. The experiment is in good agreement with the simulated data with an error estimation of about +/- 10%.

The Experiment was restarted seven times during at different daytimes and days. The experiment is in good agreement with the simulated data with an error estimation of about +/- 10%.

In another simulation, equations (3) and (4) were used to simulate the distribution of ions in our sensor geometry. The result of this simulation is shown in figure 9. The red zone is the region where the highest concentration of ions can be found. The red arrows illustrate the side wind of 1m/s. The ions are blown away from the right plate to the left plate. Therefore, the current on the left plate increases, while the current on the right plate decreases. The electric field lines are illustrated by the golden colored lines. With very good agreement to the experiment we get 5.11  $\mu\text{A}$  on the left plate and 1.70  $\mu\text{A}$  on the right plate. Without side flow, the current on both plates is about 3.5  $\mu\text{A}$ .

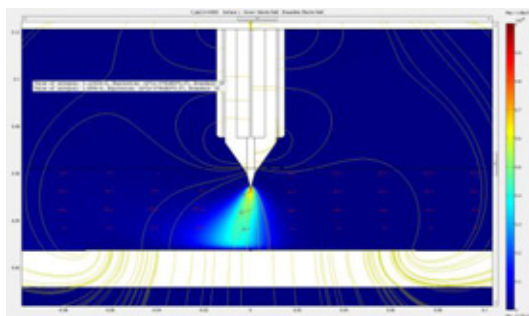


**Figure9.** Calculation of the concentration of ion in a corona current due to air flow from the side

## 7. Conclusions

A positive corona in the point-to-plane geometry was modeled using CM. The Warburg distribution of current and the current- voltage characteristic of this geometry was calculated with good agreement to the experiment. Additionally, the distribution of ions was determined using the Convection and Diffusion application mode.

## 8. References

- [1] A.Goldman, E. R. (1978, September).Current distribution in the negative corona discharge in air. *Proceedings in the fifth GD*, (pp. 87-91).  
 [2] Adrian Aeta, Z. K. (2005).Laplacian

Approximation of the Warburg distribution. *J.Electrostatics* **63** , pp. 143-145.

- [3] F. Pontiga, C. S. (2002, October). Physiochemical Modeling of negative corona in oxygen: the effect of boundaries. *Annual Report Conference on Electrical Insulation and Dielectric Phenomena*, Cancun Mexico , pp. 797-800.  
 [4] J.Q.Feng. (1999). Application of Galerkin Finite element method with Newtonian iterations In computing steady-state solutions of unipolar charge current in corona devices. *J.compt.Phys.* **151** , pp. 969-989.  
 [5] K.J.McLean, I. (1987). Calculation of the rod plane voltage current characteristics using the saturated current density equation and Warburgs law. *IEE Proc.* **134** (10, part A), (pp. 784-788).  
 [6] M.Goldman, A.Goldman and R.S.Sigmond (1985). The corona discharge, its properties and specific uses. *Pure and Appl. Chem.* Vol 57, No.9 pp.1353-1362  
 [7] R.Morrow. (1997). The theory of positive Glow corona. *J.Phys.D: Appl.Phys* **30** , pp. 3099-3114.  
 [8] R.S.Sigmond. (1978). Corona Discharges, in: Meeks, J.D. Craggs (Eds.), *Electrical Breakdown in Gases* pp.319-384. Chichester: Wiley.  
 [9] R.S.Sigmond. (1982).Simple approximate Treatment of unipolar space charge-dominated coronas: the Warburg law and the saturation current. *J.Appl. Phys.* **53** (2) , pp. 891-898.  
 [10] S.Barth and S. Z. Modeling Ion Motion in a Miniaturized Ion Mobility Spectrometer (2008, November), *Proceedings Comsol Conference 2008*, Hannover Germany.  
 [11] Warburg, E. (1927). Über die stille Entladung in Gasen: *Handbuch der Physik* **vol.14** pp. 149-170  
 [12] , Zdenek Kucerovsky, William D. Greason, Adrian Ieta, Corona Impedance in a pin to plate geometry *Journal of Electrostatics* **50** (2001) 147-157  
 [13], A. Küchler, *Hochspannungstechnik*, p 137. VDI Verlag, Düsseldorf (1996)

## 9. Acknowledgements

We want to thank our colleagues and engineers in our lab in Altheim that supported this work with great and youthful enthusiasm: DI Manfred Huber, Andreas Priewasser, DI Michael Stroi and Ing. Stefan Steidl.

## 10. Appendix

### 10.1 Kaptzov assumption

In an example we show how to implement the so called Kaptzov assumption. (After having reached the corona onset voltage of about 3000 Volts, the electric field in the forehead of the needle will not rise anymore, although the voltage is increased, because of equilibrium between a cloud of charges in front of the needle and the electric field.) In figure10 the electric field and space charge distribution for positive corona as reported in literature is shown [13]. As one can see, the actual electric field is lower than the Laplace field, therefore this space charge distribution was assumed to fulfill the Kaptzov assumption.

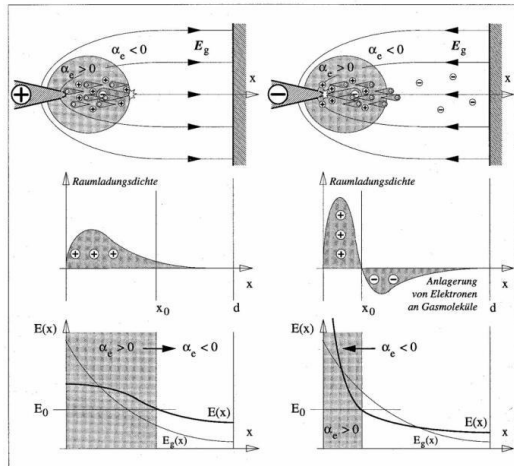


**Figure10.** Charge densities and electric field for positive corona (left side) and negative corona (right side) discharge according to the Maxwell theory and law of superposition.[13]

### 10.2 Modeling with Comsol Multiphysics

In our example we have a needle with a diameter of 0.3 mm, 8 mm length and 50  $\mu\text{m}$  radius of curvature. We tried to find a proper charge density distribution to reproduce the results depicted in figure10. We simulated a typical corona pin to plate setup, consisting of a steel needle as anode and two copper plates as collector. The voltage at the tip varied between 8000 V and 10000 V.

For the model shown in figures 11 to 13 we used a charge density function of the form

$$\rho = A \cdot r \cdot \exp(-B \cdot r),$$

A and B have been used as fitting parameters, r is the distance to the tip of the needle. Although we used the recommended charge distribution, we were not able to reproduce the results shown in figure10. Changing the parameters A and B resulted in different 2D profiles of charge density. Although the shape of our charge distribution (shown in figure11) looked like shape for positive coronas shown in figure10, the electric field did not agree with literature, which predicts a slowly decreasing electric field close to the needle. In the case of positive corona discharge a local minimum and maximum of E(x) is found close to the tip, which is shown in figure12.

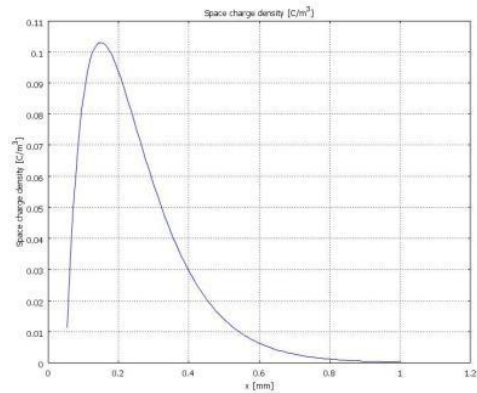


**Figure11.** Charge density distribution used for calculating the electric field.

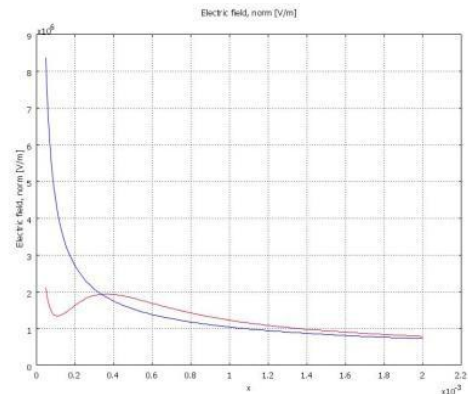


**Figure12.** The blue line shows the electric field along needle axis without the positive charged cloud in front of the tip, the red line shows the electric field considering a positive space charge as shown in figure11.

A 2-D plot of the electric field is shown in figure13.

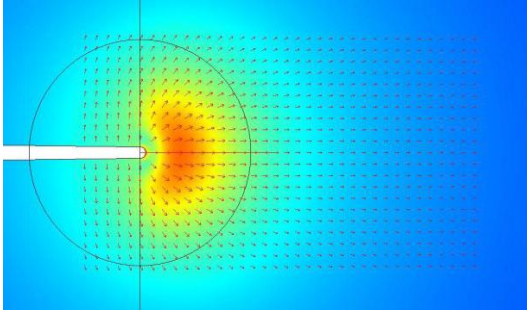


**Figure13.** Simulation of the electric field assuming a space charge density according to [13].

### 10.3 Conclusion

Using Comsol Multiphysics we could demonstrate, that the electric field of a positive corona does not have the simple shape as suggested by text books.